Received 30 September 2020; revised 25 November 2020; accepted 2 December 2020. Date of publication 15 December 2020; date of current version 4 February 2021.

Digital Object Identifier 10.1109/JXCDC.2020.3045074

Understanding the Continuous-Time Dynamics of Phase-Transition Nano-Oscillator-Based Ising **Hamiltonian Solver**

SOURAV DUTTA[®] (Member, IEEE), ABHISHEK KHANNA (Student Member, IEEE), and SUMAN DATTA (Fellow, IEEE)

> Electrical Engineering Department, University of Notre Dame, Notre Dame, IN 46556 USA CORRESPONDING AUTHOR: S. DUTTA (sdutta4@nd.edu)

This work was supported in part by Applications and Systems driven Center for Energy-Efficient Integrated NanoTechnologies (ASCENT), one of six centers in Joint University Microelectronics Program (JUMP), sponsored by the Defense Advanced Research Projects Agency (DARPA), and in part by the NSF-SRC SemiSynBio.

This article has supplementary downloadable material available at https://doi.org/10.1109/JXCDC.2020.3045074, provided by the authors.

ABSTRACT Many combinatorial optimization problems can be mapped onto the ground-state search problem of an Ising model. Exploiting the continuous-time dynamics of a network of coupled phasetransition nano-oscillators (PTNOs) allows building an Ising Hamiltonian solver for obtaining optimum or near-optimum solution with a large speed-up over discrete-time iterative digital hardware. Here, we provide insights into the continuous-time dynamics of such a PTNO-based Ising Hamiltonian solver. We highlight the formation of stable attractor states in the phase space of the coupled PTNO network using secondharmonic injection locking (SHIL) that corresponds to the minima of the Ising Hamiltonian. We show that the emergent synchronized dynamics of the PTNO network is maximized near the critical point of oscillator phase bistability beyond which the dynamics is limited by freeze-out effects. Such dynamical freeze-out severely limits the performance of the PTNO-based Ising solver from obtaining the global optimum. We highlight an improvement in the success probability of reaching the ground state by introducing an annealing scheme with linearly increasing SHIL amplitude compared with a constant SHIL. Finally, we estimate the "effective temperature" of the PTNO-based Ising solver by comparing it with the Markov chain Monte Carlo simulations. The PTNO-based Ising solver behaves like a low-temperature Ising spin system, indicating its effectiveness for optimization tasks.

INDEX TERMS Injection-locked oscillators, Ising machine, nonlinear dynamical systems, optimization.

I. INTRODUCTION

♦ OMBINATORIAL optimization problems have immense real-world applications, including financial portfolio optimization, bioinformatics, drug discovery, cryptography, operations research, resource allocation, satellite-based target tracking, and trajectory and route planning [1]-[4]. However, many of these problems belong to the nondeterministic polynomial time (NP)-hard or NP-complete complexity class, indicating an exponential increase in the resources required to solve the problem as the problem size increases. Interestingly, many such problems can be reformulated into another physics problem—finding the ground state of an Ising model [4]–[6]. The Ising Hamiltonian describes the energy of a spin system with discrete binary spins states σ and a symmetric coupling matrix J and is given by $H = -\sum_{i=1}^{N} J_{ij}\sigma_i\sigma_j$. Exact algorithms, such as branchand-bound, can take a prohibitively large time to reach a guaranteed ground state of the Ising model for a reasonable problem size of a few hundred spins. As such, heuristic algorithms and stochastic methods, such as semidefinite program [7], breakout local search [8], metropolis algorithm (MA) [9], and simulated annealing [10], have been proposed that can provide approximate solutions (optimum or suboptimal solutions) in a reasonable timeframe.

An exciting new avenue of research has been focused on building the Ising Hamiltonian solvers using physical systems called Ising machines that hold the promise of providing solutions much faster than an iterative algorithm running on a digital computer. Recently, various proposals for building such special-purpose Ising machines using a variety of techniques have been put forward. These include superconducting qubits and trapped ion-based quantum computing and quantum annealing [11]-[13], digital and mixed-signal complementary metal-oxide-semiconductor (CMOS) annealers

This work is licensed under a Creative Commons Attribution 4.0 License. For more information, see https://creativecommons.org/licenses/by/4.0/

[14]–[19], photonic Ising machine [20], and coherent networks of degenerate optical parametric oscillators [21], [22]. Qubit-based quantum annealers add a high overhead in terms of cost and complexity due to cryogenic operating conditions. The optical coherent Ising machine proves to be competitive when compared against quantum annealer [23] but requires a long fiber ring cavity for implementing Ising spins. In addition, it requires an extremely fast and powerhungry field-programmable gate array (FPGA) for implementing coupling in a measure-and-feedback scheme [22]. The CMOS-based annealing machines use techniques, such as near-memory [17] or in-memory [24] computing, to reduce the memory bottleneck and improve the energy-efficiency and speed of the optimization solver. Such CMOS-based annealers have greatly improved upon the original Simulated Annealing algorithm with parallel spin update algorithms [17] that reduce the time and energy to the solution. However, even with parallel spin updates, each update step in a digital annealer requires several hundreds of clock cycles to calculate the change in Ising energy per spin-flip through multiplyand-accumulate (MAC) operations and compare the change to a random number to implement a probabilistic spin flip.

In contrast, in this work, we utilize the notion of using a continuous-time dynamical system (CTDS) to solve optimization problems. Using a CTDS approach to solve a combinatorial optimization problem involves setting up the CTDS appropriately such that the stable attractor state of the system represents the solution of the problem. Hence, as the system evolves in time through energy minimization, it can dynamically locate the global minima. The fundamental advantage in the CTDS approach compared with a digital system comes from the inherently distributed nature and highly parallel processing capability based on the continuous physical interaction between compute elements. This allows the CTDS to dynamically find the ground-state or near-optimum solution with immense speed-up compared with a sequentially working digital computer. Recently, there have been several proposals to build a CTDS using CMOS oscillators, such as LC [25] or ring oscillators [19]. In contrast, we focus on utilizing ultralow-power phase-transition nano-oscillators (PTNOs) for building a CTDS that is extremely energyefficient compared with LC or ring oscillators [26]–[28].

A PTNO-based CTDS relies on emulating the Ising Hamiltonian through its own "energy" function [28], [29]. Briefly describing, a PTNO consists of a two-terminal phase-transition hysteretic device in series with a transistor. Recently, a prototypical PTNO using vanadium dioxide (VO₂) has been experimentally demonstrated. A schematic of the PTNO considered in this work is shown in Fig. 2(a). The working principle of the VO₂-based PTNO has been reported elsewhere [27], [29], [30]. Below the insulator-to-metal (IMT) phase-transition temperature and under zero external electric fields or current, VO₂ shows insulating behavior. Upon applying an electric field across the two terminals of the device, the material undergoes an abrupt change in phase from insulating to the metallic state. The hysteretic phase transition is reflected as an abrupt hysteretic current–voltage

(I-V) characteristic of the device. Pairing a transistor in series with the VO₂ device such that the load line passes through the unstable region of the I-V curve, self-sustained oscillations can be obtained.

An overview of using such a PTNO-based Ising solver is shown in Fig. 1. The real-world problems are first mapped onto the ground-state search problem of an Ising model [4]–[6]. As shown in Fig. 1, the Ising problem is represented as a graph problem where the nodes represent binary spin states and the adjacency matrix is defined by the Ising interaction or coupling matrix J. In the corresponding PTNO-based Ising solver, spins are represented by the bistable electronic phases of the PTNOs. The Ising interaction can be realized using passive electrical elements. Particularly, it has been shown that resistive coupling is equivalent to ferromagnetic interaction (J = +1) and capacitive coupling emulates antiferromagnetic interaction (J = -1) [28], [29]. The temporal dynamics of the PTNO network is dictated by energy minimization. Hence, if the Ising energy can be represented by the "energy" function of the network, then, as the network evolves in time, it can dynamically reach the global or local minima of the Ising model. As shown in Fig. 1, this ground-state search can be further improved by exploiting the inherent stochasticity of the PTNOs and introducing annealing schemes as described later.

While both experimental as well numerical simulations have highlighted a clear advantage of PTNO-CTDS-based Ising solver over other aforementioned proposals in terms of time-and energy-to-solution [28], [29], a deeper understanding of the inherent dynamics of the PTNO network is still remaining. In this work, we present a detailed analysis of the continuous-time dynamics of the PTNO network as it evolves toward the lowest energy state. We use experimentally calibrated numerical simulations to highlight the impact of second-harmonic injection locking (SHIL) on the dynamics of the PTNO network. While the synchronized dynamics is maximized just beyond the critical point of phase-bistability, further increasing the SHIL amplitude causes freeze-out of the oscillator phases. Such dynamical freeze-out can severely limit the ability of the network to reach the ground state. We highlight a performance improvement by introducing an annealing scheme with time-varying SHIL amplitude instead of a constant SHIL strength. We also shed light on an open question regarding the "effective temperature" of the PTNO-based Ising solver. By comparing with Markov chain Monte Carlo (MCMC) simulations, we show that our Ising solver behaves like a low-temperature Ising spin system, thus indicating its effectiveness in solving optimization problems.

II. CONTINUOUS-TIME DYNAMICS AND NUMERICAL SIMULATION FRAMEWORK OF PTNO-BASED ISING SOLVER

We start by describing the PTNO network using the dynamical systems theory. A dynamical system is represented by a change in the state of the system x as a function of time t. Without loss of generality, a CTDS can be described by the time evolution of state x as $\frac{dx(t)}{dt} = g(x)$, where g can volume 6, NO. 2, DECEMBER 2020

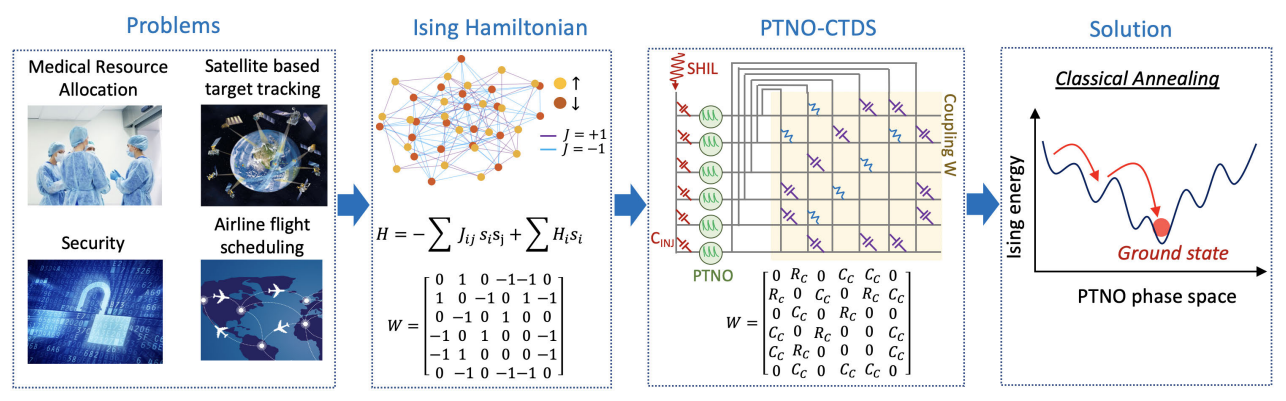


FIGURE 1. Illustrative overview of a PTNO-based Ising solver. Various real-world problems combinatorial optimization problems are mapped onto the ground-state search problem of an Ising model. The Ising Hamiltonian H is defined by the spins σ_i and a symmetrical interaction or coupling matrix J. This can be mapped onto the PTNO-based Ising solver where the spins are represented by the bistable electronic phases of the PTNOs. The Ising interaction matrix J is mapped onto coupling matrix W for the PTNO network and is realized using passive electrical elements. Resistive coupling is equivalent to ferromagnetic interaction (J = +1) and capacitive coupling emulates antiferromagnetic interaction (J = -1). The dynamics of the PTNO network is dictated by energy minimization. Hence, if the Ising energy can be represented by the "energy" function of the network, then, as the network evolves in time, it can dynamically reach the global or local minima of the Ising model. The ground-state search can be further improved by exploiting the inherent stochasticity of the PTNOs and introducing classical annealing.

be a linear or a nonlinear function describing the system. The continuous-time dynamics of our PTNO network can be described in terms of the oscillator phases. Particularly, since we consider the scenario of injection locking, we can invoke a generalized version of Adler's equation (Gen–Adler) [31] to describe the phase difference θ between the oscillator and the injection locking signal. A schematic of the PTNO with a sinusoidal injection locking signal $S_{\rm inj} = V_{\rm inj} \sin(2\pi f_{\rm inj}t)$ is shown in Fig. 2(a). The injection locking signal is applied across a capacitance $C_{\rm INJ}$. The PTNO dynamics is described by [28]

$$\frac{d\theta(t)}{dt} = -(f_{\text{inj}} - n_H f_o) + K_{\text{inj}}^H \int_0^{2\pi} \xi(\theta(t) + \vartheta) \cos(\vartheta) d\vartheta$$
(1)

where n_H is the *n*th harmonic of the PTNO and $K_{\rm inj}^H = 2\pi n_H f_o f_{\rm inj} C_{\rm inj} V_{\rm inj}$. The first term describes the frequency mismatch between $V_{\rm out}$ and $S_{\rm inj}$, which contributes to phase slipping. The second term captures the excess phase generated over 1 oscillation cycle due to the injection locking signal. It depends on the phase delay due to $S_{\rm inj}$ and is described in terms of the perturbation-projection-vector (PPV) ξ . The PPV is the phase response of the PTNO to an impulse current input normalized to the amount of injected charge and the oscillator frequency and is calculated numerically using a SPICE circuit simulation. The details of the PPV calculation are given in [28]. The corresponding "energy" or the Lyapunov function is then obtained following the equation of a gradient system [32] and is given by:

$$\frac{d\theta(t)}{dt} = -\frac{\partial E(\theta)}{\partial \theta}.$$
 (2)

Thus, the "energy" of a single injection-locked oscillator is given by [28]

$$E(\theta) = (f_{\text{inj}} - n_H f_0)\theta - K_{\text{inj}}^H \int_0^\theta \int_0^{2\pi} \xi(\phi + \vartheta) \cos(\vartheta) d\vartheta d\phi.$$
(3)

The first energy term is due to the frequency mismatch that creates an overall bias in the energy landscape. However, this being a linear term does not introduce any new valleys or peaks in the energy landscape. The second term describes the interaction between $S_{\rm inj}$ and PTNO. Equation (1) can predict the existence of stable phases locked between the PTNO and the injection locking signal when $(d\theta(t))/(dt) = 0$. These also correspond to stable minima or attractor states in the energy landscape obtained from (3).

We numerically solve (1) to simulate the continuous-time dynamics of a single PTNO subjected to injection locking. The corresponding energy landscape is obtained by numerically solving (3). In our simulations, the IMT transition voltage V_{IMT} was considered as 0.7 V, and a $V_{\text{DD}} = 1 \text{ V}$ was used in our simulations. The total capacitance of the VO₂ device was assumed to be 200 fF, while the metallic and insulating resistances were 2 and 100 k Ω , respectively. An injection locking capacitance $C_{inj} = 1$ fF was used. This resulted in an operating frequency of $f_0 = 160 \text{ MHz}$ in our simulations. The PTNOs exhibit inherent stochasticity during the abrupt phase transition between the insulator and metallic phase, occurring twice in every oscillation cycle. Such stochasticity of the PTNO is manifested as the oscillator jitter noise and is replicated in our simulations by adding a Gaussian phase noise twice every oscillation cycle. We solve the resultant stochastic version of (1) numerically using the Euler-Maruyama method. Unless mentioned, we use an oscillator-period jitter of 0.5%.

When $V_{\rm inj}=0$, the PTNO is freely running. Fig. 2(b-i) shows the simulated voltage output waveform $V_{\rm out}$ recorded over multiple runs. The corresponding oscillator phase θ , measured with respect to a reference sinusoidal signal of the same frequency f_0 , shows a uniform probability distribution over the entire phase space, as shown in Fig. 2(c-i). The "energy" function of the PTNO stays flat, as shown in Fig. 2(c-i). Interestingly, when the injection locking signal is

VOLUME 6, NO. 2, DECEMBER 2020 157

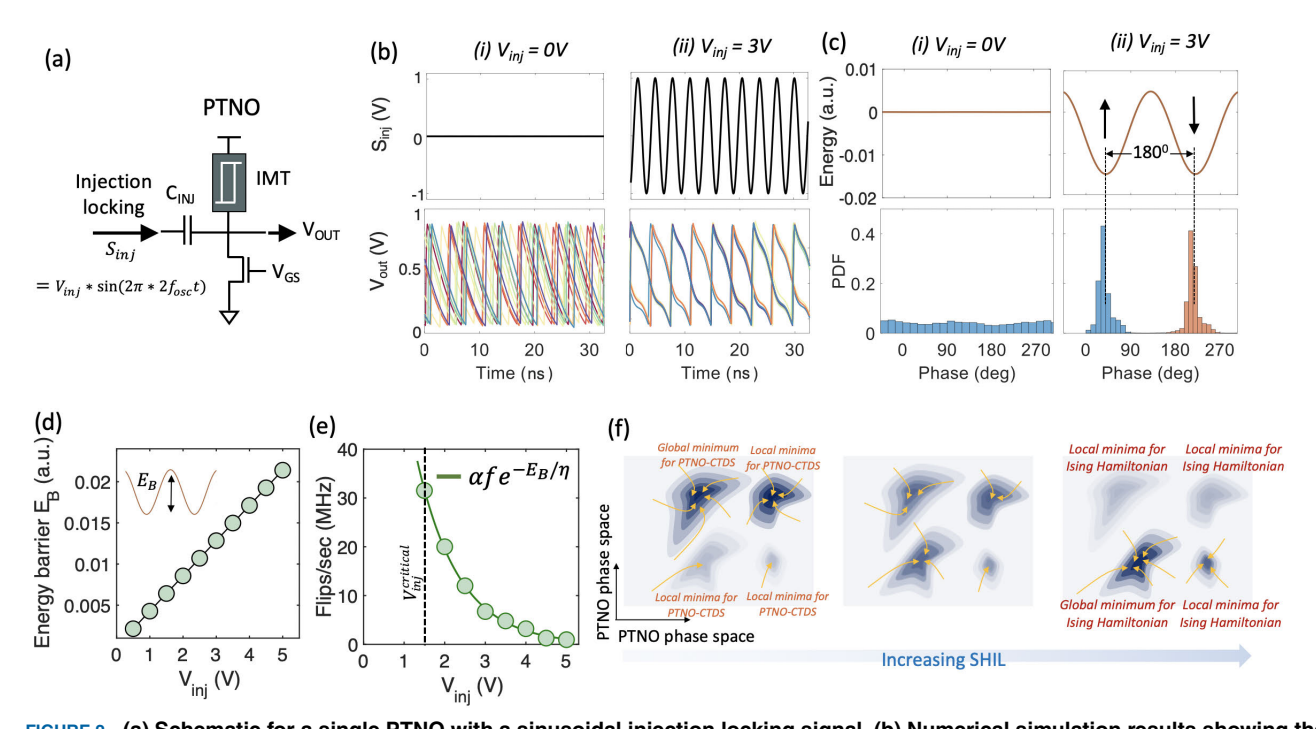


FIGURE 2. (a) Schematic for a single PTNO with a sinusoidal injection locking signal. (b) Numerical simulation results showing the output voltage waveforms of the PTNO for an applied SHIL signal. Two scenarios of (i) no injection locking signal ($V_{inj} = 0$ V) and (ii) with SHIL signal ($V_{inj} = 3$ V) are shown. SHIL allows the creation of bistable oscillator phases emulating Ising spin. (c) Calculated energy landscape of the PTNO (i) with ($V_{inj} = 0$ V) and (ii) without ($V_{inj} = 3$ V) SHIL. The application of SHIL creates a double-energy landscape, highlighting equiprobable and bistable oscillator phases separated by 180°. (d) Modulation of the energy barrier of the double-well energy landscape with V_{inj} . (e) Decrease in stochastic fluctuation of the oscillator phase with increasing V_{inj} . (f) Illustration showing the evolution of the complex energy landscape for a coupled PTNO network with increasing amplitude of the SHIL signal. Usually, the attractor state with the lowest energy for the PTNO network without the SHIL and the global minimum of the Ising Hamiltonian do not coincide. However, as the amplitude of the SHIL is increased, the desired attractor state of the PTNO network corresponding to the lowest energy of the Ising Hamiltonian becomes the global minimum.

applied at twice the frequency of the oscillator, $f_{\rm inj} \approx 2f_0$, also known as the SHIL condition, the simulated oscillator output waveform shows both in-phase and out-of-phase configurations when recorded over multiple runs, as shown in Fig. 2(b-ii). The corresponding probability distribution of the oscillator phase exhibits a double-Gaussian distribution highlighting equiprobable and bistable phase portraits, as shown in Fig. 2(c-ii). This bistability allows us to emulate the Ising spin in the electrical domain, where $\theta = 40^{\circ}$ represents up-spin, i.e., = +1, and $\theta = 220^{\circ}$ represents down-spin, i.e., $\sigma = -1$. These two peaks obtained using numerical simulations are also consistent with the predicted equilibrium points $\theta \cong 0.2\pi$ and $\theta \cong 1.2\pi$ obtained using $\frac{d\theta(t)}{dt} = 0$. This is also supported by the energy landscape calculated using (3), which gives a double-well energy landscape that results in a double Gaussian distribution in the phase space (assuming zero frequency mismatch).

There exists a critical amplitude of the injection signal $V_{\rm inj}^{\rm critical}$ below which no stable solution exists. Fig. 2(d) shows the modulation of the energy barrier of the double-well energy landscape with $V_{\rm inj}$. As the strength of $V_{\rm inj}$ increases, the depth of the double-well energy landscape increases. The modulation of the energy barrier is also associated with the stochastic fluctuation of the phase of the oscillator [28]. Such stochastic fluctuations, measured in terms of flips-persecond, are essential to escaping local minima, as will be

discussed later. Fig. 2(e) shows that, close to the critical voltage $V_{\rm inj}^{\rm critical}$, the bistable oscillator phases exhibit constant temporal fluctuation with a very low dwell time and high flips/s. As the strength of $V_{\rm inj}$ increases, the depth of the double-well energy landscape (or energy barrier E_B) increases, resulting in a decrease in the number of flips per second. The decrease in flips/s with increasing $V_{\rm inj}$ accurately follows the characteristics of Arrhenius's relation $\alpha f e^{-E_B/\eta}$, where f is the fundamental frequency of the oscillator, α is the fitting parameter, and η is the stochastic noise in the PTNO. This characteristic of reduction in the temporal fluctuations of the oscillator's phase with increasing amplitude of injection locking signal proves to be a key knob toward performing classical annealing in our hardware.

Using a similar mathematical treatment, as mentioned earlier, we can describe the continuous-time dynamics of a network of coupled PTNOs. It has been shown that PTNOs can be coupled using simple passive electrical elements, such as resistance and capacitance. The nature of coupling, resistance or capacitance, dictates the tendency of the PTNOs to remain in-phase or out-of-phase with each other [27], [33], [34]. Recently, this was further exploited to establish that resistive or capacitive coupling can indeed establish ferromagnetic or antiferromagnetic interaction in a PTNO-based Ising Hamiltonian solver [28], [29]. In the following, we describe the continuous-time dynamics of such a coupled PTNO network

158 VOLUME 6, NO. 2, DECEMBER 2020

subjected to SHIL and incorporating resistive or capacitive coupling

$$\frac{d\theta_{i}(t)}{dt} = -(f_{\text{inj}} - n_{H}f_{o,i}) + K_{\text{inj},i}^{H} \int_{0}^{2\pi} \xi_{i}(\theta_{i}(t) + \vartheta)\cos(\vartheta)d\vartheta$$
$$+ f_{0} \sum_{j=1, j\neq i}^{N} \int_{0}^{2\pi} \xi_{i}(\theta(t) + \vartheta)I_{\text{osc},j}d\vartheta. \quad (4)$$

Note the additional third term describing the coupling interaction energy between pairs of oscillators. $I_{\text{osc},j} = C_{C,j}(dV_{\text{osc}},j)/(dt)$ or $= -(V_{\text{osc},j})/(R_{C,j})$ depending on capacitive coupling (using $C_{C,j}$) or resistive coupling (using $R_{C,j}$), respectively. The corresponding "total energy" function of the PTNO network is

$$E(\vec{\theta}) = \sum_{i=1}^{N} (f_{\text{inj}} - n_H f_0) \theta_i$$

$$-K_{\text{inj}}^H \sum_{i=1}^{N} \int_0^{\theta_i} \int_0^{2\pi} \xi_i (\phi + \vartheta) \cos(\vartheta) d\vartheta d\phi$$

$$-f_0 \sum_{i,j=1, i \neq j}^{N} \int_0^{\theta_i} \int_0^{2\pi} \xi_i (\phi + \vartheta) I_{\text{osc},j} d\vartheta d\phi. \quad (5)$$

To simulate the dynamics of the PTNO-based Ising solver, (4) is solved numerically using the Euler–Maruyama method. Throughout our simulation, we use coupling capacitance $C_C = 30$ fF. The corresponding "energy" function is obtained by solving (5). In general, when the amplitude of SHIL is less than the critical voltage $V_{\rm inj}^{\rm critical}$, the oscillator phases are not constrained into only binarized phases, and the coupled PTNO network can contain multiple attractor states. A schematic of such a complex phase space in the continuous phase space domain is illustrated in Fig. 2(f), exhibiting four attractor states: one global and three local minima. Note that, usually, the attractor state with the lowest energy for the PTNO network without the SHIL and the global minimum of the Ising Hamiltonian do not coincide. However, as shown in Fig. 2(f), by increasing the amplitude of the SHIL signal beyond $V_{\rm inj}^{\rm critical}$, binarization of the oscillator phases occurs, and the desired attractor state of the PTNO network corresponding to the lowest energy of the Ising Hamiltonian becomes the global minimum. Thus, this ensures that, as the PTNOs settle in the appropriate phase configuration, they also minimize the Ising Hamiltonian. However, while the SHIL facilitates the binarization of the oscillator phases and creation of the Ising attractor states, the amplitude of the SHIL has a crucial influence on the dynamics of the PTNO network and is discussed in detail next.

III. DYNAMICAL FREEZE-OUT EFFECT AND IMPACT ON GROUND-STATE SEARCH

To better understand the PTNO dynamics and the impact of the SHIL amplitude during the ground-state search process, we start by analyzing a 2-D square lattice structure with periodic boundary conditions for which the ground state is already known [35]. We consider a lattice of size 40×40 VOLUME 6, NO. 2, DECEMBER 2020

with nearest-neighbor antiferromagnetic coupling (J = -1). For this problem, the ground state corresponds to an alternating arrangement of spin-up and spin-down states in a checkerboard pattern. We use capacitive coupling in our simulation for mimicking the antiferromagnetic interactions. An SHIL signal of constant amplitude and greater than $V_{\rm inj}^{\rm critical}$ is applied through the simulation time to maintain binarized oscillator phases. Fig. 3(a) shows the time evolution of the 2-D domain structure for all the 1600 PTNOs in the Ising solver. The different snapshots correspond to different oscillation cycles, and the top and bottom figures correspond to different SHIL amplitudes. Note that the PTNO phases are multiplied with a checkerboard pattern that transforms the problem into a ferromagnetic case, making it easier to visualize the evolution of domains. Thus, blue domains correspond to one antiferromagnetic configuration $(\uparrow\downarrow\uparrow\downarrow\dots\uparrow\downarrow)$, and yellow domains correspond to the opposite antiferromagnetic configuration $(\downarrow\uparrow\downarrow\uparrow)$... $\downarrow\uparrow$). We start the simulations from a randomized spin state. As the PTNO network evolves in time, the oscillator phases start to reorganize, as shown in Fig. 3(b). This causes the corresponding artificial spins in the 2-D lattice to self-organize into domains such that one domain (say blue) grows in size, while the other domain (say yellow) shrinks in order to minimize the Ising energy of the system by reducing the total boundary between two domains where unfavorable configurations ($\uparrow \uparrow$ or $\downarrow \downarrow$) exist. In Fig. 3(a) and (b), the temporal evolution of the domains and the oscillator phases for two different SHIL amplitudes are shown. For an SHIL amplitude of $V_{\rm inj} = 3.5$ V, the evolution of domains continues until the network reaches the ground state. This is also reflected in the temporal evolution of the Ising energy in Fig. 3(c), where, for $V_{\text{inj}} = 3.5 \text{ V}$, the network reaches the ground-state energy. However, as shown in Fig. 3(a), a higher SHIL amplitude of $V_{\text{inj}} = 6 \text{ V}$ causes the creation of smaller domains with a large number of domain walls. The temporal dynamics remain very slow, and ultimately, the network exhibits a freeze-out where the domain evolution stops and remains in this frozen state as its final configuration. This is also reflected in the temporal evolution of the phases of the oscillations showing reduced dynamics and frozen behavior of the network. This indicates a significant influence of the SHIL amplitude on the continuous-time dynamics of the PTNO-based Ising solver.

Fig. 3(c) shows the temporal evolution of the Ising energy for different SHIL amplitudes. For a low SHIL amplitude of $V_{\rm inj}=2.5$ V, the network evolves to a higher Ising energy state compared with the ground state. This is because, for smaller SHIL amplitude, the network gets stuck in an attractor state that does not correspond to the global minimum of the Ising Hamiltonian [similar to the scenario explained in Fig. 2(d)]. On the other hand, arbitrarily increasing the amplitude of the SHIL signal causes a freeze-out effect, forcing the network to evolve to a final configuration having a higher Ising energy, as shown in Fig. 3(c). There remains a close interplay between the SHIL amplitude and the stochasticity present in the system. Fig. 3(d) shows the success probability of reaching the ground-state energy configuration for varying

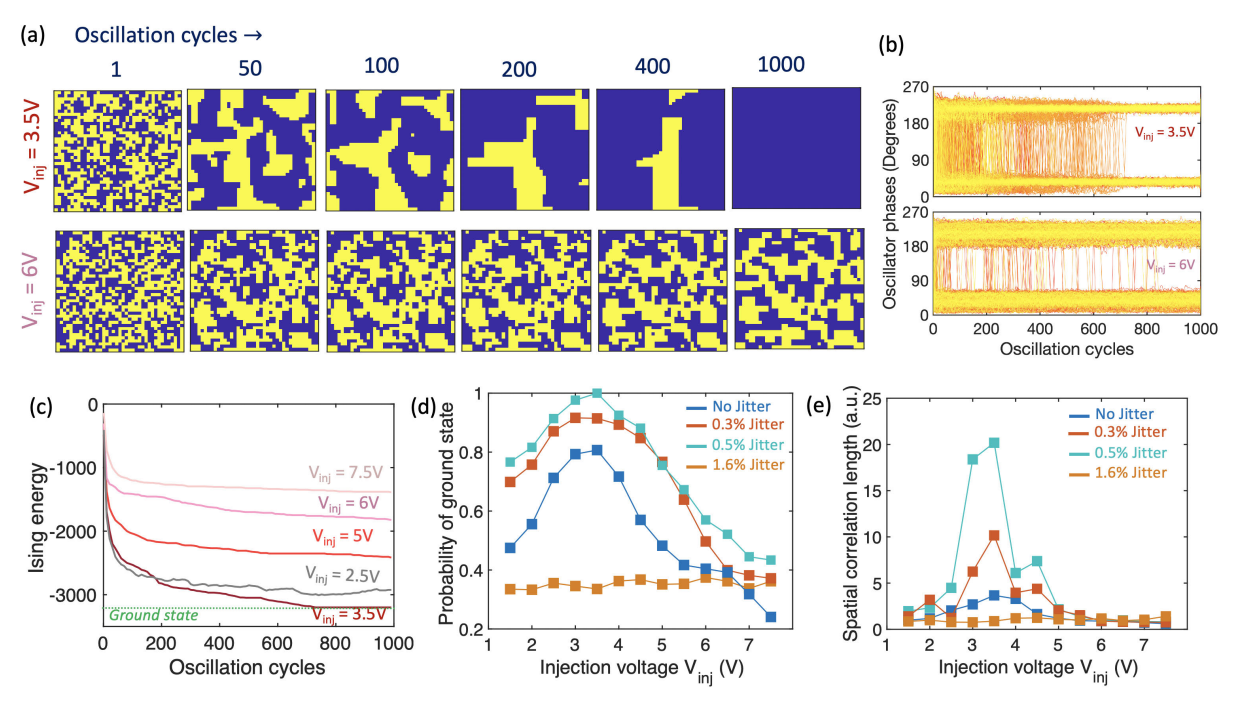


FIGURE 3. (a) and (b) Snapshots of the temporal evolution of the domains and oscillator phases during the ground-state search for two different SHIL amplitudes. For V_{inj} close to the critical value, the PTNO network is able to reach the ground state. However, there remains an optimum V_{inj} for which the ground-state search is maximized. For a high V_{inj} , freeze-out effect is seen. (c) Temporal evolution of the Ising energy for different SHIL amplitudes. (d) Probability of reaching the ground state for varying SHIL amplitude and different oscillator jitter noise. (e) Spatial correlation length as a function of SHIL amplitude and different oscillator jitter noises.

SHIL amplitude and different oscillator jitter noises. For a given noise of 0.5% jitter, we see that, far from $V_{\rm ini}^{\rm critical}$, the final state of the network reaches only 46% of the groundstate energy before freeze-out, while, just above $V_{\rm inj}^{\rm critical}$, the network can reach the ground-state energy. This sheds light on the fact that the dynamics of the PTNO network is maximum near the critical point of oscillator phase bistability. Stochasticity also plays a critical role in affecting the likelihood of the oscillator network to escape the local energy minima and reach the global optimum. Too little stochasticity (oscillator jitter) means that the system gets stuck in local minima and is not able to jump out to reach the global minimum. On the other hand, a very large amount of intrinsic noise would cause the system to jump out of the global energy minimum configuration even at the highest SHIL, leading to lower success probability. By varying the amount of oscillator jitter noise, we found that a 0.5% jitter was the ideal amount of noise to achieve maximum success probability. As will be discussed later, the success probability of reaching the ground state for other nonplanar complex graphs also shows a similar trend with varying SHIL amplitude and a peak just beyond the critical point. Note that the range of optimum SHIL amplitude required is quite narrow, as shown in Fig. 3(d). This can be further improved by introducing annealing schemes and is discussed later. Similar dynamical freeze-out effects have been reported in coherent networks of degenerate optical parametric oscillators (coherent Ising machine) used to minimize the Ising energy [36], [37].

Another key metric to quantify the dynamics of the PTNO network for such a 2-D lattice is to calculate the spatial correlation length. The spatial correlation length λ

is calculated by fitting the 2-D autocorrelation function of the spin configuration with an exponential function $e^{r/\lambda}$, where r is the spatial coordinate. It is seen in Fig. 3(e) that the spatial correlation length increases drastically around the optimal SHIL amplitude, just beyond the critical point. This is because, for suboptimal SHIL amplitude, larger domains are formed that contributes to increase the correlation among domains. As the SHIL amplitude is further increased beyond the optimal regime, the dynamical freeze-out effect sets in creating a large number of domains of smaller size and a smaller correlation length. The requirement for optimum stochasticity (oscillator jitter noise) is also seen in Fig. 3(e), where the spatial correlation length is maximum for 0.5% oscillator jitter. Overall, this sheds light on the fact that the PTNO-based Ising solver needs to be operated with optimum stochasticity and optimal SHIL amplitude in order to avoid the freeze-out effect and enable an effective ground-state search.

IV. ESTIMATING EFFECTIVE TEMPERATURE OF PTNO-BASED ISING SOLVER

It has been shown that the amplitude of SHIL plays a crucial role during the ground-state search and can be utilized as a mechanism to perform classical annealing to obtain progressively better solutions [28], [29]. This has a close resemblance with the simulated annealing algorithm that utilizes a decaying temperature parameter to obtain progressively improved solution [10]. Thus, it is informative to estimate the "effective temperature" of the PTNO-based Ising solver under different SHIL amplitudes. For this, we compare the results of our PTNO network for the 2-D square lattice with

160 VOLUME 6, NO. 2, DECEMBER 2020

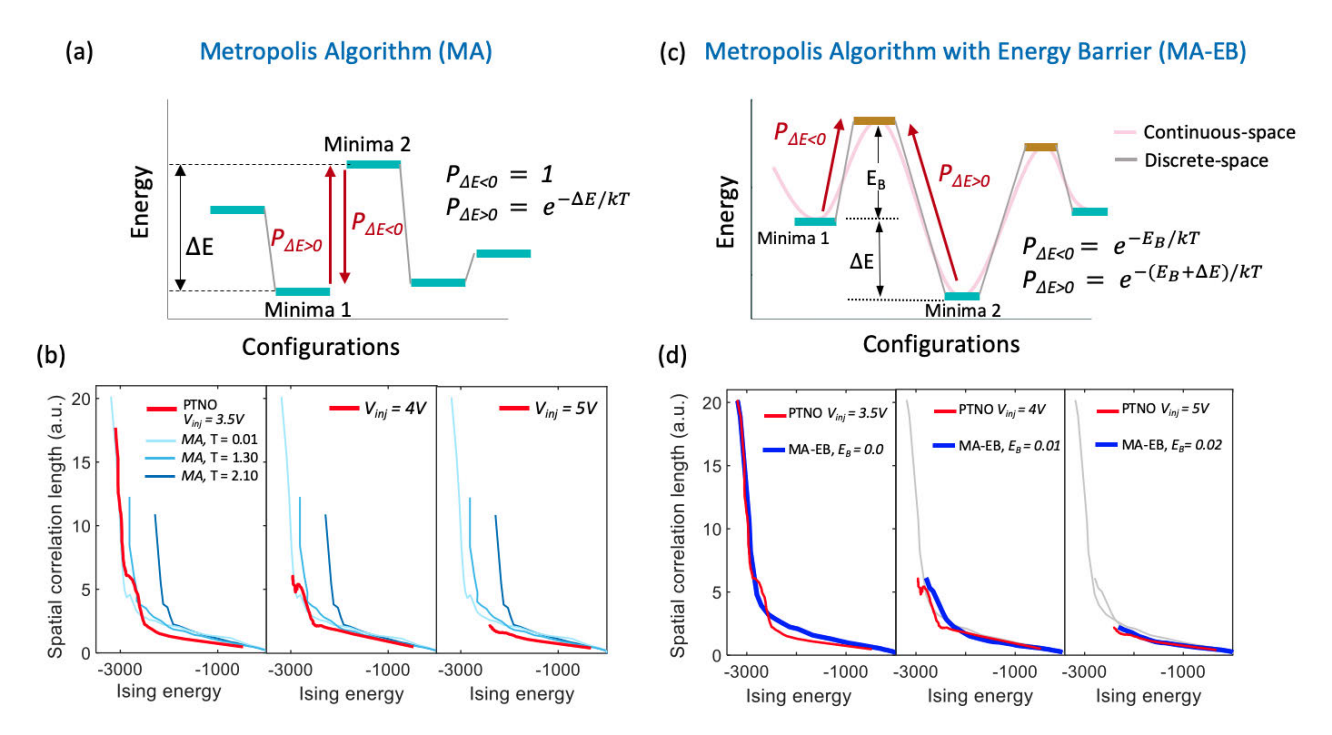


FIGURE 4. (a) Schematic of the MA used for MCMC simulations of the 2-D square lattice. (b) Temporal evolution of the Ising energy and correlation length during the ground-state search for both MCMC simulations at different temperatures and PTNO-based Ising solver for different SHIL amplitudes. This establishes that different SHIL amplitudes do not emulate varying temperature parameters. Instead, the dynamics of the PTNO-based Ising solver mimics a low-temperature Ising spin system. (c) Schematic of the proposed MA-EB. (d) Temporal evolution of the Ising energy and correlation length for both MCMC simulations with different energy barriers E_B and PTNO-based Ising solver for different SHIL amplitudes. The excellent match validates the role of the SHIL in introducing an energy barrier in the energy landscape rather than behaving as the temperature parameter.

MCMC simulations using a MA at different temperatures [9]. As illustrated schematically in Fig. 4(a), the MA involves flipping of a randomly selected single spin in each iteration and comparing the energy of the new configuration with the previous one. If the energy gets reduced by ΔE , the spin flip is accepted with a probability of $P_{\Delta E < 0} = 1$. On the other hand, if the energy increases by ΔE , the spin flip is, nonetheless, accepted with a probability given by the Boltzmann factor $P_{\Delta E > 0} = e^{-\Delta E/kT}$, where k is the Boltzmann factor and T is the temperature.

To perform a quantitative comparison, we follow the methodology delineated by [36] where we track the temporal evolution of the Ising energy and the correlation length. We compare the trajectories in the phase space of correlation length versus the Ising energy for both our PTNO-based Ising solver and the MCMC simulation. It is seen from the MCMC simulations that, for low T = 0.01, the correlation length initially remains low and drastically increases as the Ising energy approaches the ground state. For higher temperatures of T = 1.3 and 2.1, the trajectory deviates significantly from the low-temperature behavior where the correlation length remains higher for a given Ising energy. Interestingly, we see that all the trajectories of the PTNO-based Ising solver for different SHIL amplitude align with the trajectory corresponding to T = 0.01 of the MCMC simulation. This establishes the fact that, although a temporally varying SHIL amplitude can be used to perform classical annealing through controlling the temporal fluctuation in the oscillator phases, SHIL does not emulate the temperature parameter of the simulated annealing algorithm. It also indicates that dynamics of the PTNO-based Ising solver mimics a low-temperature Ising spin system and, thus, can be effectively used for solving optimization problems [36].

To further shed light on the mechanism behind the freezeout effect, we mimic the continuous-time and continuousspace dynamics of the PTNO-based Ising solver with a discrete-time and discrete-space MA augmented with an energy barrier (MA-EB), as shown in Fig. 4(c). Note that this is a simplified discrete-state interpretation of the energy landscape, which qualitatively matches with the continuousspace energy landscape shown in Fig. 4(c) around the energy minima points but remains effective in explaining the freezeout effect. As mentioned earlier, an increase in the amplitude of the SHIL causes an increase in the depth of the individual energy minima, while the difference between the minima ΔE remains the same, as shown in Fig. 4(c). This, in turn, introduces an additional energy barrier E_B . Thus, in contrast to the MA, here if the oscillator phases try to stochastically rearrange themselves to a newer configuration that reduces the energy by ΔE , the subsequent probability will be given by $P_{\Delta E < 0} = e^{-E_B/kT}$. This is because the PTNO network still needs to overcome the additional energy barrier E_B introduced by the SHIL. On the other hand, the probability that the oscillator phases stochastically rearrange themselves to a newer configuration that increases the energy by ΔE is given by $P_{\Delta E > 0} = e^{-(E_B + \Delta E)/kT}$. Thus, with an increasing

VOLUME 6, NO. 2, DECEMBER 2020 161

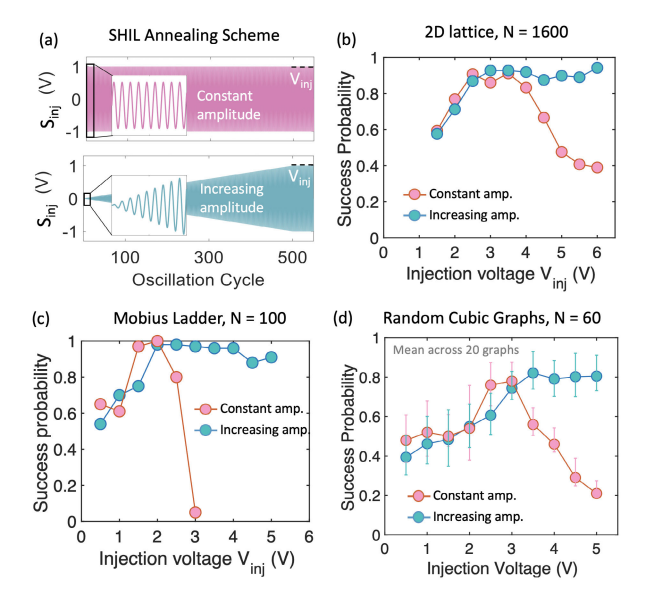


FIGURE 5. (a) Illustration of the two different schemes of applying the SHIL signal. (b)–(d) Success probability of finding the ground state as a function of $V_{\rm inj}$ for three different graphs. Each simulation is rerun for 100 trials to calculate the success probability. For random cubic graphs, we ran the simulations for 20 different representative graphs. This illustrates that using an annealing scheme can widen the parameter space for optimizing the performance and even enhance the probability of reaching the ground state as the complexity of the problem increases.

amplitude of SHIL, E_B increases, which contributes to the oscillator phases getting trapped in local minima and causing the freeze-out effect. We also compare the trajectories in the phase space of correlation length versus the Ising energy for our PTNO-based Ising solver and MCMC simulations using the new MA-EB algorithm. As shown in Fig. 4(d), they show an excellent match, thus validating the role of the SHIL in introducing an energy barrier in the energy landscape rather than behaving as the temperature parameter of a simulated algorithm. In fact, the role of the temperature parameter is rather mimicked by the inherent stochastic noise of the PTNOs.

V. PERFORMANCE IMPROVEMENT OF PTNO-BASED ISING SOLVER WITH ANNEALING

Next, we extend our analysis to calculating the success probability of finding the ground state for three different graphs: 1) a 2-D lattice of size 40×40 with periodic boundary condition; 2) a 100-node Mobius Ladder graph; and 3) 20 randomly generated representative 60-node cubic graphs of degree 3, all with antiferromagnetic interaction (capacitive coupling). We consider two different schemes of applying the SHIL signal, as shown in Fig. 5(a). For each data point in Fig. 5(b)–(d), the simulation was rerun for 100 trials to calculate the success probability. For a constant SHIL, the amplitude is kept constant throughout the simulation. For an increasing SHIL, the amplitude is linearly increased from 0 to the desired $V_{\rm inj}$. As shown in Fig. 5(b)–(d), the success probability of obtaining the ground state increases as the SHIL amplitude $V_{\rm inj}$ increases from suboptimal to an optimal

value. Beyond the optimal point, a constant SHIL scheme shows a monotonic decline in the performance of the Ising solver. Hence, for the constant SHIL scheme, the parameter space of SHIL amplitude that optimizes the performance of the PTNO-based Ising solver is narrow. Note that, for a constantly applied SHIL, the solver performs the stochastic search in the solution space that may provide a limited success probability for complicated problems.

In contrast, when resorting to a linear anneal scheme with linearly increasing SHIL amplitude, the performance of the Ising solver shows negligible degradation even if $V_{\rm inj}$ is increased beyond the optimal regime. Thus, using a linear anneal scheme widens the parameter space for optimizing the performance. This is because, as the amplitude of SHIL is slowly varied from the suboptimal to the optimal regime, the continuous-time dynamics of the PTNO network allows an effective exploratory search of the state space and allows obtaining a progressively better solution. As the amplitude of SHIL is further increased linearly beyond the optimal regime, the exploratory dynamics of the network is curtailed with a reduction of spin flips per second. Overall, our Ising solver is able to reach a success probability of over 95% for both the SHIL schemes. Interestingly, the average success probability obtained over 20 random cubic graphs by annealing is higher than that obtained by performing the stochastic search with a constant SHIL, as shown in Fig. 5(d). We further investigate the sensitivity of success probability on non-idealities such as oscillator noise and frequency variation (see supplementary information for details).

VI. CONCLUSION

We provide crucial insight into the continuous-time dynamics of a PTNO-based Ising Hamiltonian solver. Through experimentally calibrated numerical simulations, we delineate the notion of creating attractor states in the phase space of the coupled PTNO network that will correspond to the minima of the Ising Hamiltonian. Through comprehensive analysis, we establish that the dynamics of the PTNO network is maximum just beyond the critical point of oscillator phase bistability. This can be effectively exploited to perform an exploratory search for the ground state in the solution space. This is in line with a general concept witnessed in dynamical systems that emergent complex dynamics occur near a criticality point [38]. A great example is the spin dynamics at the subcritical, critical, and supercritical temperatures, exhibiting secondorder ferromagnetic-paramagnetic phase transition. Only at the critical temperature, the system shows highly correlated domains. We also highlight SHIL-induced dynamic freezeout effects that curtail the dynamics of the solver and hinder the ground-state search. Subsequently, we provide a pathway toward improving the performance of the Ising solver by utilizing annealing schemes. Finally, we provide an estimation of the "effective temperature" of the PTNO-based Ising solver by comparing it with MCMC simulations and highlight a low-temperature Ising spin behavior exhibited by our PTNO-based Ising solver.

162 VOLUME 6, NO. 2, DECEMBER 2020

REFERENCES

- M. R. Garey and D. S. Johnson, Computers and Intractability, vol. 174. San Francisco, CA, USA: Freeman, 1979.
- [2] G. Cornuejols and R. Tütüncü, Optimization Methods in Finance, vol. 5. Cambridge, U.K.: Cambridge Univ. Press, 2006.
- [3] D. B. Kell, "Scientific discovery as a combinatorial optimisation problem: How best to navigate the landscape of possible experiments?" *BioEssays*, vol. 34, no. 3, pp. 236–244, Mar. 2012.
- [4] G. Bass, C. Tomlin, V. Kumar, P. Rihaczek, and J. Dulny, "Heterogeneous quantum computing for satellite constellation optimization: Solving the weighted k-clique problem," *Quantum Sci. Technol.*, vol. 3, no. 2, Apr. 2018, Art. no. 024010.
- [5] A. Lucas, "Ising formulations of many NP problems," Frontiers Phys., vol. 2, p. 15, Feb. 2014.
- [6] F. Glover, G. Kochenberger, and Y. Du, "Quantum bridge analytics I: A tutorial on formulating and using QUBO models," 4OR, vol. 17, no. 4, pp. 335–371, Dec. 2019.
- [7] M. X. Goemans and D. P. Williamson, "Improved approximation algorithms for maximum cut and satisfiability problems using semidefinite programming," *J. ACM*, vol. 42, no. 6, pp. 1115–1145, Nov. 1995.
- [8] U. Benlic and J.-K. Hao, "Breakout local search for the max-cutproblem," Eng. Appl. Artif. Intell., vol. 26, no. 3, pp. 1162–1173, Mar. 2013.
- [9] N. Metropolis, A. W. Rosenbluth, M. N. Rosenbluth, A. H. Teller, and E. Teller, "Equation of state calculations by fast computing machines," *J. Chem. Phys.*, vol. 21, no. 6, pp. 1087–1092, Jun. 1953.
- [10] S. Kirkpatrick, C. D. Gelatt, and M. P. Vecchi, "Optimization by simulated annealing," *Science*, vol. 220, no. 4598, pp. 671–680, May 1983.
- [11] M. W. Johnson et al., "Quantum annealing with manufactured spins," Nature, vol. 473, no. 7346, pp. 194–198, May 2011.
- [12] S. Boixo et al., "Evidence for quantum annealing with more than one hundred qubits," *Nature Phys.*, vol. 10, no. 3, pp. 218–224, Mar. 2014.
- [13] K. Kim et al., "Quantum simulation of frustrated Ising spins with trapped ions," Nature, vol. 465, no. 7298, pp. 590–593, Jun. 2010.
- [14] S. Tsukamoto, M. Takatsu, S. Matsubara, and H. Tamura, "An accelerator architecture for combinatorial optimization problems," *Fujitsu Sci. Tech. J.*, vol. 53, no. 5, pp. 8–13, Sep. 2017.
- [15] M. Yamaoka, C. Yoshimura, M. Hayashi, T. Okuyama, H. Aoki, and H. Mizuno, "24.3 20k-spin Ising chip for combinational optimization problem with CMOS annealing," in *IEEE Int. Solid-State Circuits Conf.* (ISSCC) Dig. Tech. Papers, Feb. 2015, pp. 1–3.
- [16] T. Takemoto, M. Hayashi, C. Yoshimura, and M. Yamaoka, "2.6 A 2 × 30k-spin multichip scalable annealing processor based on a processing-in-memory approach for solving large-scale combinatorial optimization problems," in *IEEE Int. Solid-State Circuits Conf. (ISSCC) Dig. Tech. Papers*, Feb. 2019, pp. 52–54.
- [17] K. Yamamoto et al., "7.3 STATICA: A 512-spin 0.25M-weight full-digital annealing processor with a near-memory all-spin-updates-at-once architecture for combinatorial optimization with complete spin-spin interactions," in *IEEE Int. Solid-State Circuits Conf. (ISSCC) Dig. Tech. Papers*, Feb. 2020, pp. 138–140.
- [18] Y. Su, H. Kim, and B. Kim, "31.2 CIM-spin: A 0.5-to-1.2 V scalable annealing processor using digital compute-in-memory spin operators and register-based spins for combinatorial optimization problems," in *IEEE Int. Solid-State Circuits Conf. (ISSCC) Dig. Tech. Papers*, Feb. 2020, pp. 480–482.
- [19] I. Ahmed, P.-W. Chiu, and C. H. Kim, "A probabilistic self-annealing compute fabric based on 560 hexagonally coupled ring oscillators for solving combinatorial optimization problems," in *Proc. IEEE Symp. VLSI Circuits*, Jun. 2020, pp. 1–2.

- [20] D. Pierangeli, G. Marcucci, and C. Conti, "Large-scale photonic Ising machine by spatial light modulation," *Phys. Rev. Lett.*, vol. 122, no. 21, May 2019, Art. no. 213902.
- [21] P. L. Mcmahon et al., "A fully programmable 100-spin coherent Ising machine with all-to-all connections," Science, vol. 354, no. 6312, pp. 614–617, Nov. 2016.
- [22] T. Inagaki et al., "A coherent Ising machine for 2000-node optimization problems," Science, vol. 354, no. 6312, pp. 603–606, Nov. 2016.
- [23] R. Hamerly et al., "Experimental investigation of performance differences between coherent Ising machines and a quantum annealer," Sci. Adv., vol. 5, no. 5, May 2019, Art. no. eaau0823.
- [24] F. Cai *et al.*, "Power-efficient combinatorial optimization using intrinsic noise in memristor Hopfield neural networks," *Nature Electron.*, vol. 3, no. 7, pp. 409–418, Jul. 2020.
- [25] T. Wang and J. Roychowdhury, "OIM: Oscillator-based ising machines for solving combinatorial optimisation problems," in *Proc. Int. Conf. Unconv. Comput. Natural Comput.* Springer, 2019, pp. 232–256.
- [26] N. Shukla et al., "Synchronized charge oscillations in correlated electron systems," Sci. Rep., vol. 4, May 2014, Art. no. 4964.
- [27] S. Dutta et al., "Programmable coupled oscillators for synchronized locomotion," Nature Commun., vol. 10, no. 1, pp. 1–10, Jul. 2019.
- [28] S. Dutta et al., "An Ising Hamiltonian solver using stochastic phase-transition nano- oscillators," 2020, arXiv:2007.12331. [Online]. Available: https://arxiv.org/abs/2007.12331
- [29] S. Dutta, A. Khanna, J. Gomez, K. Ni, Z. Toroczkai, and S. Datta, "Experimental demonstration of phase transition nano-oscillator based Ising machine," in *IEDM Tech. Dig.*, Dec. 2019, pp. 37.8.1–37.8.4.
- [30] S. Dutta, A. Khanna, W. Chakraborty, J. Gomez, S. Joshi, and S. Datta, "Spoken vowel classification using synchronization of phase transition nano-oscillators," in *Proc. Symp. VLSI Technol.*, Jun. 2019, pp. T128–T129.
- [31] P. Bhansali and J. Roychowdhury, "Gen-Aadler: The generalized Adler's equation for injection locking analysis in oscillators," in *Proc. Asia South Pacific Design Automat. Conf. (ASP-DAC)*, no. 2, Jan. 2009, pp. 522–527.
- [32] J. L. van Hemmen and W. F. Wreszinski, "Lyapunov function for the Kuramoto model of nonlinearly coupled oscillators," *J. Stat. Phys.*, vol. 72, pp. 145–166, Jul. 1993.
- [33] A. Parihar, N. Shukla, S. Datta, and A. Raychowdhury, "Synchronization of pairwise-coupled, identical, relaxation oscillators based on metal-insulator phase transition devices: A model study," *J. Appl. Phys.*, vol. 117, no. 5, 2015, Art. no. 054902.
- [34] A. Parihar, N. Shukla, M. Jerry, S. Datta, and A. Raychowdhury, "Vertex coloring of graphs via phase dynamics of coupled oscillatory networks," *Sci. Rep.*, vol. 7, no. 1, pp. 1–19, 2017.
- [35] L. Onsager, "Crystal statistics. I. A two-dimensional model with an orderdisorder transition," *Phys. Rev.*, vol. 67, nos. 3–4, p. 117, Feb. 1944.
- [36] F. Böhm et al., "Understanding dynamics of coherent Ising machines through simulation of large-scale 2D Ising models," *Nature Commun.*, vol. 9, no. 1, pp. 1–9, Nov. 2018.
- [37] T. Inagaki, K. Inaba, R. Hamerly, K. Inoue, Y. Yamamoto, and H. Takesue, "Large-scale Ising spin network based on degenerate optical parametric oscillators," *Nature Photon.*, vol. 10, no. 6, pp. 415–419, Jun. 2016.
- [38] D. R. Chialvo, "Emergent complex neural dynamics," *Nature Phys.*, vol. 6, no. 10, pp. 744–750, Oct. 2010.

. . .